Simulation of Scattering Properties of Gels

A. Moussaïd* and P. N. Pusey

Department of Physics and Astronomy, The University of Edinburgh, Mayfield Road, Edinburgh, EH9 3JZ, Scotland

J. J. M. Slot and J. G. H. Joosten

Department PAC, DSM Research, P.O. Box 18, NL-6160 MD Geleen, The Netherlands

Received July 23, 1998; Revised Manuscript Received February 16, 1999

ABSTRACT: Brownian dynamics simulations of a simple model of a polymer gel were performed to investigate the conditions under which gels show nonergodicity, the presence of frozen density fluctuations which do not relax completely, and to explore possible connections between nonergodicity and the existence of density fluctuations of large spatial extent which are observed in many real gels. The gel was modeled by a random two-dimensional network of springs, formed by bond dilution of a regular triangular lattice. Scatterers located at the nodes of the network moved in Brownian motion. Average scattered intensities and time correlation functions of the intensities were calculated for different gel connectivities and spring constants. These well-defined model systems exhibited both large-scale inhomogeneities and nonergodicity, but no unambiguous connection between the two was found. Nevertheless, in some cases scattering behavior very similar to that of real gels was observed.

1. Introduction

Polymer gels consist of random cross-linked networks of polymer molecules dissolved in a liquid. Such a gel is a classic example of a "soft solid", being easily deformed by a weak stress, yet recovering its initial shape on release of the stress due to the elasticity conferred by the permanent cross-links. The structure and dynamics of gels can be probed by scattering techniques. In early dynamic light scattering (DLS) experiments it was discovered that the electric field amplitude of the scattered light frequently contains both fluctuating and static, or nonfluctuating, components.[1,2] In much of this early work, the static components were considered to be caused by "uninteresting" inhomogeneities of spatial scale comparable to the wavelength of light and much larger than the typical distance between cross-links. DLS measurements were analyzed in terms of a "heterodyne mixing" between the static and fluctuating fields. The "interesting" dynamics of the latter were interpreted through a continuum viscoelastic model of the gel.[3]

More recently, Pusey and van Megen[4] have pointed out that gels are intrinsically nonergodic and that even a gel without large-scale inhomogeneities can show static scattering. Nonergodicity follows from the fact that the scatterers, or polymer segments, are localized in space by the cross-links:[4,5] they are able to perform only limited Brownian motions about fixed average positions. A particular sample of the gel is thus trapped in a restricted region of phase space. The static scattering results from the associated "frozen-in" concentration fluctuations. A question then arises: Is it possible to distinguish experimentally between these two sources of static scattering, large-scale inhomogeneities and intrinsic nonergodicity? Recent DLS experiments on poly(acrylamide) and poly(acrylic acid) gels have not been able to provide an unambiguous answer.[6,7] Therefore, we have turned to computer simulation, calculating the scattering properties of a two-dimensional gel modeled by a random elastic network. These simulations form the subject of this paper.

A two-dimensional model "gel" is generated by random bond dilution of a triangular lattice of springs.[8] Scatterers located at the nodes of this random lattice undergo Brownian motion. The scattering properties are calculated for various degrees of bond dilution and different spring constants. This well-defined model system exhibits behavior similar in several respects to that of real gels, showing both large-scale inhomogeneities and nonergodicity. However, we did not find an unambiguous connection between the inhomogeneities and the nonergodicity. Under some conditions homogeneous gels can be intrinsically nonergodic; in other cases gels with large-scale inhomogeneities appear to be fully dynamic.

For simplicity throughout this paper we will call these random networks "gels". We emphasize, however, that the model system is still far from representing a real polymer gel. The most severe simplification is the neglect of the structure and interactions of the polymer chains. Thus, the calculated scattering properties are only realistic on spatial scales much larger than the lattice parameter or mesh size (which is, in fact, the regime probed in real gels by light scattering; see section 2.2). A more serious consequence is that excluded-volume interactions between monomers on the polymer chains are neglected. The importance of excluded-volume effects, and the osmotic pressure associated with excluded volume, on the structure of gels has recently been emphasized by Panyukov and Rabin[5] (see sections 2.4 and 4 for further discussion). Nevertheless, despite these strong limitations of the model and the complexity of real gels, we believe the work reported here to be a worthwhile first step toward more realistic simulations.

2. Model and Simulations

2.1. The Model Gel. Initially we performed a few simulations on a three-dimensional model gel. To obtain

10.1021/ma981159n CCC: $18.00
Published on Web 05/14/1999

Table 1. Distribution of Vertex Connectivities (C = 0, 1, 2, ..., C_{max}) for Examples of Gels with Maximum Connectivities C_{max} = 4 and 5

connectivity	fraction $C_{max} = 4$	fraction $C_{max} = 5$
0	0.00	0.00
1	0.08	0.00
2	0.12	0.015
3	0.28	0.065
4	0.52	0.28
5		0.64

accurate results without excessively long simulations, these were limited to quite small systems. Therefore, in this paper we consider only two-dimensional gels. We note, however, that the limited results obtained with the three-dimensional system were qualitatively similar to those reported here.

The two-dimensional model gel was constructed as follows. We start with a regular $N \times N$ triangular lattice with lattice parameter a. The connectivity, or coordination, of each vertex is 6, and each link consists of a harmonic spring with spring constant κ. The random configuration is obtained by bond dilution[8] of the original regular array. Each of the $3N^2$ bonds is considered in random sequential order and is removed when at least one of the connectivities of the adjacent vertexes is larger than some preset maximum value C_{max}. This process is continued until no vertex has connectivity greater than C_{max}. It is a correlated process in that the local environment of a given bond determines whether it will be cut. The end result is a graph with vertexes having connectivities ranging from 0 to C_{max}. The connected part of this graph corresponds to the gel and the rest to the sol fraction. Each spring mimics a polymer segment with entropic elasticity. In the simulation the polymeric strands behave as phantom chains, able to pass through one another. Periodic boundary conditions are applied in both directions.

Table 1 shows the distribution of vertex connectivities for typical examples with $C_{max} = 5$ and 4, the values used in the simulations. For $C_{max} = 4$, the fraction of unconnected, or "monomer", vertexes is zero, and the fraction of vertexes corresponding to free dimers is 6.4×10^{-3}; the remainder of vertexes with connectivity 1 correspond to "dangling ends" of clusters of three or more vertexes.

2.2. The Simulation Algorithm. Since, in a real gel, the typical spacing between cross-links, ~10 nm, is much smaller than the wavelength of light, each polymer segment can be regarded as a point scatterer. Thus, for simplicity in the simulation, we take the scatterers to be points, or beads, located at the vertexes of the network. The interaction of this bead−spring network with the underlying liquid is treated within a Langevin or Brownian dynamics framework, with the friction and noise forces acting on the vertexes. Hydrodynamic interactions between the vertexes are neglected.

In the high-friction or overdamped limit, where inertial terms can be neglected, the equation of motion for vertex j can be written

$$\dot{\underline{r}}_j(t) = -\frac{1}{\zeta}\nabla_j U[\underline{r}^N(t)] + \sqrt{\frac{2k_B T}{\zeta}}\underline{B}_j(t) \qquad (1)$$

where $\underline{r}_j(t)$ is the position of vertex j at time t, $\underline{r}^N(t)$ represents the positions of all the vertexes, ζ is the friction coefficient of a single vertex, k_B is Boltzmann's constant, T is the temperature, and $\underline{B}_j(t)$ describes the Brownian force, having properties

$$\langle \underline{B}_j(t)\rangle \equiv \underline{0}, \quad \langle B_{j\alpha}(t)\, B_{k\beta}(t')\rangle \equiv \delta_{jk}\delta_{\alpha\beta}\delta(t - t') \qquad (2)$$

where α, β represent Cartesian components. The potential energy U of the system is given by

$$U[\underline{r}^N(t)] = \frac{1}{2}\kappa\sum_{j=1}^{N_V}\sum_{\delta} b_j^{\delta}|\underline{r}_{j+\delta} - \underline{r}_j|^2 \qquad (3)$$

where κ is the spring constant, $N_V = N^2$ is the number of vertexes, and the second sum runs over the bonds of vertex j, the variable b_j^{δ} being 1 if a spring is present and 0 otherwise. Equation 1 can be integrated over a short time step Δt, to give the Brownian dynamics algorithm[9]

$$\underline{r}_j(t+\Delta t) - \underline{r}_j(t) = -\frac{1}{\zeta}\nabla_j U[\underline{r}^N(t)]\Delta t + \sqrt{\frac{2k_B T}{\zeta}}\Delta\underline{W}_j(\Delta t) \qquad (4)$$

where the random term $\Delta\underline{W}_j(\Delta t)$ is chosen from a Gaussian distribution with zero mean and variance

$$\langle \Delta\underline{W}_j(\Delta t)\, \Delta\underline{W}_k(\Delta t)\rangle = \mathbf{1}\delta_{jk}\Delta t \qquad (5)$$

The natural unit of time is

$$t_0 = \frac{a^2}{D_0} \qquad (6)$$

where the diffusion constant of a vertex is $D_0 = k_B T/\zeta$; t_0 is 4 times the time taken by a free vertex to diffuse over one lattice spacing a. In most of the simulations reported below we took the time step $\Delta t = 5 \times 10^{-3} t_0$. In this time, a free vertex would diffuse a distance $(\sqrt{2}/10)a$ (see eqs 4 and 5). In the following we define the dimensionless spring constant

$$K = \frac{\kappa a^2}{k_B T} \qquad (7)$$

Thus, when $K = 1$, a spring stretched by one lattice constant has potential energy $^1/_2\kappa a^2$ equal to one-half the thermal energy $k_B T$.

2.3. Light Scattering. To simulate light scattering, each vertex is considered to be a scatterer with unit scattering strength. Each configuration $\{\underline{r}^N(t)\}$ will lead, within the first Born approximation, to a scattered field

$$E(\underline{Q},t) = \sum_{j=1}^{N_V}\exp[i\,\underline{Q}\cdot\underline{r}_j(t)] \qquad (8)$$

where $\underline{Q}$ is the scattering vector. If the real-space triangular lattice is described by lattice vectors $\underline{a}$ and $\underline{b}$ of lengths a at angle 120° to each other, the reciprocal lattice vectors $\underline{a}^*$ and $\underline{b}^*$ have lengths $2/\sqrt{3}a$ and a mutual angle of 60°. Periodic boundary conditions require that the allowed scattering vectors are given by

$$\underline{Q} = \frac{2\pi}{N}(n_1\underline{a}^* + n_2\underline{b}^*) \qquad (9)$$

where n_1 and n_2 are integers ranging in value from $-\infty$ to $+\infty$. The magnitude $Q \equiv |\underline{Q}|$ of the scattering vector is

$$Q = \frac{4\pi}{\sqrt{3}Na}\sqrt{n_1^2 + n_1 n_2 + n_2^2} \tag{10a}$$

In what follows it will be convenient to define a dimensionless scattering vector by

$$\underline{q} = \underline{Q}a \tag{10b}$$

The scattered intensity corresponding to the field of eq 8 is given by

$$I(\underline{Q},t) = |E(\underline{Q},t)|^2 = [\sum_j \cos[\underline{Q}\cdot\underline{r}_j(t)]]^2 + [\sum_j \sin[Q\cdot r_j(t)]]^2 \tag{11}$$

The resolution of the calculation depends on the size N of the lattice or sample. The smallest scattering vector q, obtained by taking $n_1 = 1$, $n_2 = 0$ in eq 10, corresponds to the largest structure which can be studied, essentially the whole sample. In principle, there is no upper limit on q, but $q > 2\pi$ ($Q > 2\pi/a$) corresponds to structures on scales smaller than the lattice spacing which are not of interest in this study.

The quantity most easily obtained from a dynamic light scattering measurement is the normalized time-averaged intensity autocorrelation function (ICF)[4]

$$g_T^{(2)}(q,\tau) \equiv \frac{\langle I(q,0)\, I(q,\tau)\rangle_T}{\langle I(q,0)\rangle_T^2} \tag{12}$$

where, in practice, the time averages are calculated via

$$\langle I(q,0)\, I(q,\tau)\rangle_T = \frac{1}{T_E - \tau}\int_0^{T_E-\tau} I(q,t)\, I(q,t+\tau)\, \mathrm{d}t,$$
$$\langle I(q,0)\rangle_T = \frac{1}{T_E}\int_0^{T_E} I(q,t)\, \mathrm{d}t \tag{13}$$

and T_E is the duration of the measurement. The quantity of interest is usually the ensemble-averaged autocorrelation function of the scattered field amplitude, or intermediate scattering function,

$$f(q,\tau) = \frac{\langle E(q,0)\, E^*(q,\tau)\rangle_E}{\langle |E(q,0)|^2\rangle_E} \tag{14}$$

which can also be interpreted as the correlation function of density fluctuations in reciprocal space (see eq 8). For an ergodic medium, time and ensemble averages are equivalent, $g_T^{(2)}(q,\tau) = g_E^{(2)}(q,\tau)$, and $f(q,\tau)$ can be calculated from the well-known result[4]

$$f(q,\tau) = \sqrt{g_E^{(2)}(q,\tau) - 1} \tag{15}$$

However for a nonergodic medium, which contains frozen density fluctuations, the measured $g_T^{(2)}(q,\tau)$ depends on the structure, or topology, of the actual sample under study and varies from sample to sample. Then two methods can be used to obtain $f(q,\tau)$.[4] The first is to calculate ensemble averages by summing over a large number M of samples:

$$\langle I(q,0)\, I(q,\tau)\rangle_E = \frac{1}{M}\sum_{p=1}^{M}\langle I(q,0)\, I(q,\tau)\rangle_T^p,$$
$$\langle I(q)\rangle_E = \frac{1}{M}\sum_{p=1}^{M}\langle I(q)\rangle_T^p,$$
$$g_E^{(2)}(q,\tau) \equiv \frac{\langle I(q,0)\, I(q,\tau)\rangle_E}{\langle I(q,0)\rangle_E^2} \tag{16}$$

where, for example, $\langle I(q)\rangle_T^p$ represents the time-averaged scattered intensity in topology p. Equation 15 then gives $f(q,\tau)$. The second is the method of Pusey and van Megen[4,6,10] in which $f(q,\tau)$ is calculated from a single measurement of $g_T^{(2)}(q,\tau)$ and $\langle I(q)\rangle_T$ for a particular topology, combined with a measurement of the intensity $\langle I(q)\rangle_E$ averaged over an ensemble of samples:

$$f(q,\tau) = 1 + \frac{\langle I(q)\rangle_T}{\langle I(q)\rangle_E}[\sqrt{1 + g_T^{(2)}(q,\tau) - g_T^{(2)}(q,0)} - 1] \tag{17}$$

For future use we note the $\tau \to \infty$ limit of eq 17:

$$f(q,\infty) = 1 + \frac{\langle I(q)\rangle_T}{\langle I(q)\rangle_E}[\sqrt{2 - g_T^{(2)}(q,0)} - 1] \tag{18}$$

(which follows from the fact that $g_T^{(2)}(q,\infty) = 1$).

2.4. The Simulations. In early simulations we investigated approximate ways to take some account of the effects of excluded volume between the monomers constituting the polymer chains. For this bead−spring model, the most realistic method would probably be to give *all* the vertexes hard-core repulsions to prevent their overlap. However, this method proved to be far too expensive computationally. We therefore tried the more limited approaches of applying hard-core repulsions just between *connected* vertexes or giving the springs nonzero rest lengths. For large spring constants ($K = 10$) these approaches reduced the density fluctuations somewhat. For small spring constants ($K = 0.1$), where vertexes distant in the original undiluted network can overlap, they had little effect. In the end we decided that these attempts to make the model somewhat more realistic were not sufficiently effective to justify the extra time needed for computation. In the current studies, therefore, we used purely elastic networks with springs of zero rest length and vertexes without excluded volume. However, as discussed in section 1, we recognize that neglect of excluded volume seriously limits the model as a representation of real gels,[5] especially in the case of small spring constants where vertexes distant in the original network can overlap. Nevertheless, the simulations remain a legitimate test of the relationship between inhomogeneities and nonergodicity in a well-defined system.

The lattice size used was 48 × 48. Each sample, or topology, was run for typically 10^5 time steps, during which time a free vertex would diffuse about 40 lattice spacings. The time-averaged intensity $\langle I(q)\rangle_T$ and intensity correlation function $\langle I(q,0)\, I(q,\tau)\rangle_T$ were calculated from discretized versions of eq 13. The ensemble averages $\langle I(q)\rangle_E$ and $g_E^{(2)}(q,\tau)$, eq 16, were obtained from $M = 64$ separate samples. Note that, because the scatterers are assumed to be points, the ensemble-

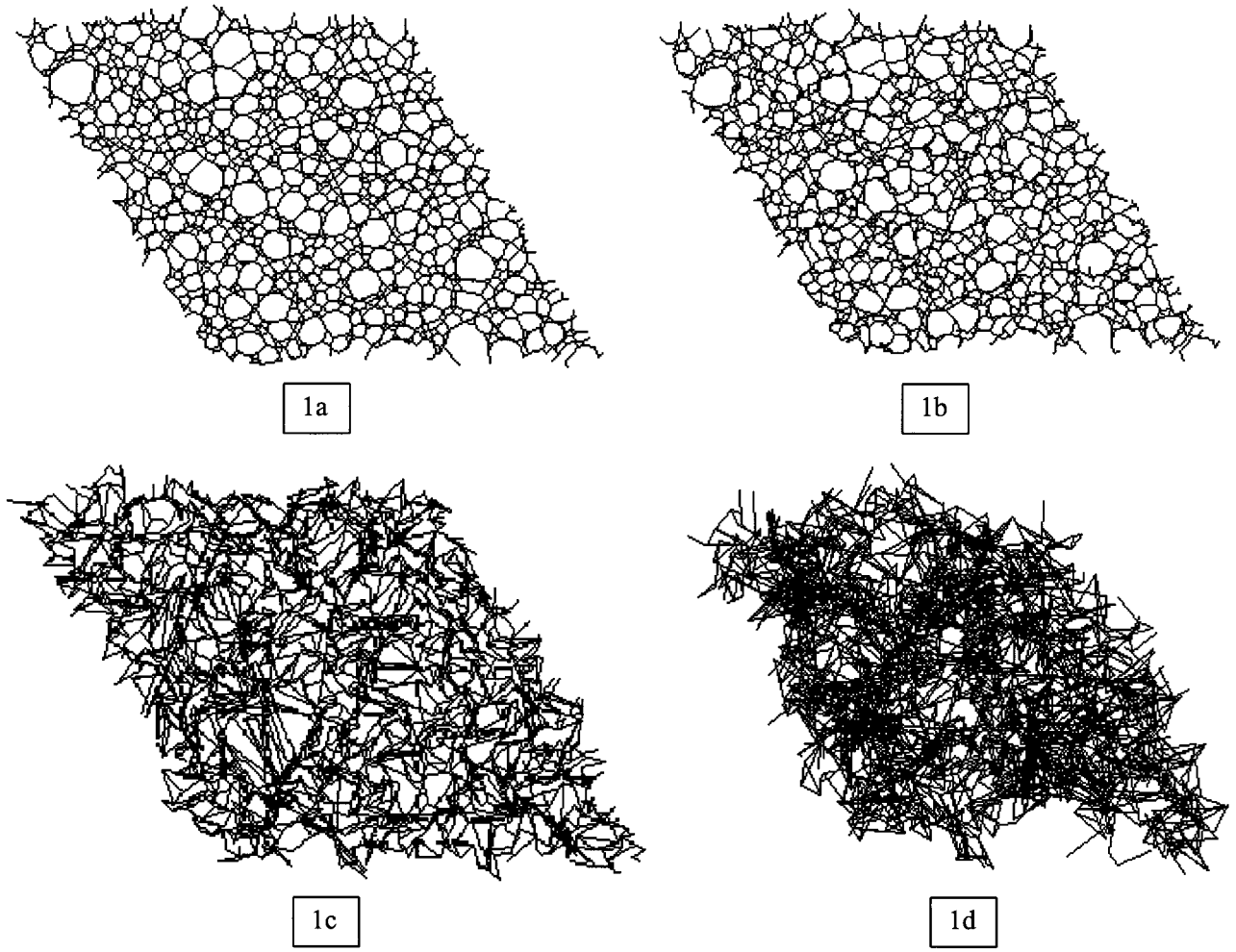

Figure 1. Representations of the real-space structure of a model gel on a 48 × 48 lattice, formed by bond dilution with maximum connectivity $C_{max} = 4$. (a) The relaxed configuration in the absence of Brownian motion. (b−d) The same gel after 10^5 time steps of Brownian motion with three different values of normalized spring constant K: (b) $K = 10$, (c) $K = 1$, and (d) $K = 0.1$. Note the similarity of the structure with strong springs (b) to the relaxed structure (a).

averaged intensity can be directly associated with the static structure factor $S(q)$ of the gel:

$$S(q) = \frac{\langle I(q)\rangle_E}{N^2} \tag{19}$$

The ensemble averaged intermediate scattering functions $f(q,\tau)$ were calculated by both methods outlined above, eqs 15 and 16, and eq 17.

There are two main sources of statistical uncertainty in the quantities calculated. First, the simulations are run for a finite number, usually $T_E = 10^5$, time steps. The relative uncertainty in time-averaged quantities such as $\langle I(q)\rangle_T$ and $g_T^{(2)}(q,\tau)$ is proportional to $\sqrt{T_C/T_E}$, where T_C is the characteristic time of fluctuations in the intensity or, roughly speaking, the decay time of $g_T^{(2)}(q,\tau)$ or $f(q,\tau)$. In Figure 3, where $T_C < 100$ time steps, we expect a relatively small uncertainty from this source, <3%. However, for calculations made at small values of the scattering vector, e.g., Figure 5, T_C is larger, and larger uncertainties are expected. Second, when ensemble averages are calculated by summing results from M samples, e.g., eq 16, the relative uncertainty is expected to be proportional to $M^{-1/2}$, with a prefactor that depends on the relative magnitude of the static scattering. For $M = 64$ and strong static scattering, uncertainties in ensemble-averaged quantities as large as 10% can be expected. Further details are given in the Appendix.

3. Results and Discussion

3.1. Structure ($C_{max} = 4$). (a) Real Space Structure. We start by considering a system with maximum connectivity $C_{max} = 4$. Figure 1a shows a particular sample of the gel, formed by bond dilution (section 2.1), which has been allowed to relax to its minimum-energy configuration in the absence of Brownian motion. The random nature of the structure is clearly evident. Figure 1b−d shows snapshots of the same sample (i.e., having the same topology of bonds) after 10^5 time steps of Brownian motion with normalized spring constants $K = 10$, 1, and 0.1, respectively. With the stiffest springs, $K = 10$ (Figure 1b), the vertexes have not moved far from their relaxed positions, and features seen in the relaxed structure are still evident after Brownian motion. However with weaker springs, $K = 1$ and $K = 0.1$, the instantaneous structures of Figure 1c,d look quite different from the relaxed structure of Figure 1a.

One observes from Figure 1 that, as the spring constant is decreased, the system develops large clusters. By looking at the structures with $K = 0.1$ as a function of time (see Figure 9) we found that these clusters were dynamic, growing, and decaying at random locations (see sections 3.2(c) and 3.3 for further

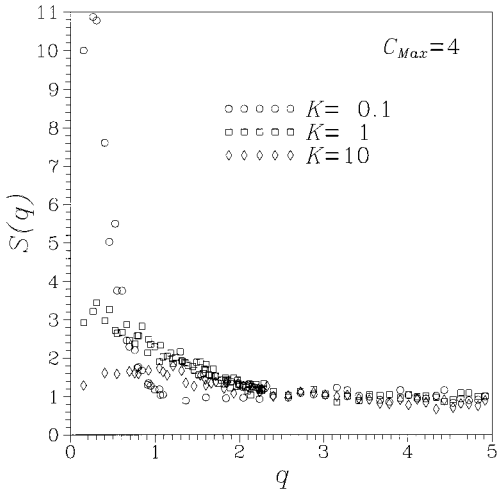

Figure 2. Ensemble-averaged structure factors $S(q)$ versus scattering vector q for gel with maximum connectivity C_{max} = 4 and indicated values of the normalized spring constant K.

discussion). The existence of these clusters is surprising at first sight; they will be discussed further in section 4. We wondered whether they might result from a "phase separation" into regions having different average connectivities. We tested this conjecture by calculating the spatial radial distribution functions of vertexes having connectivities 3 and 4 for a system with $K = 0.1$ (and $C_{max} = 4$). To within the uncertainty of the calculations, the two functions measuring autocorrelations of 3-connected and of 4-connected vertexes, as well as the 3−4 cross-correlation function, all looked the same, implying no preferential segregation by connectivity. The same calculation was repeated for a system with very low spring constant, $K = 0.001$, so that the vertexes move essentially freely throughout the simulation box. The results implied (as expected for this case) a homogeneous distribution of vertexes.

(b) Structure Factors. Figure 2 shows the ensemble-averaged structure factors $S(q)$, obtained from the ensemble-averaged intensities $\langle I(q)\rangle_E$ using eq 19 with $N = 48$, for the same three values of spring constant. For each value of dimensionless scattering vector q the ensemble averages were constructed from $M = 64$ different samples according to eq 16. Furthermore, the values of $\langle I(q)\rangle_E$ having different scattering vectors q (i.e., different values of n_1 and n_2 in eq 9), but magnitudes q (eq 10) lying between q and $q + \Delta q$, with $\Delta q = 0.1$, were summed to give a more precise estimate. Thus, for q greater than about 1 in Figure 2, where eight or more pairs of n_1 and n_2 contribute to a single data point, the values of $S(q)$ are accurate to 4% or better.

At large scattering vectors, $q > 2.5$, $S(q) \sim 1$. At low q, the structure factors increase, having the largest values for the smallest spring constant. This implies the presence of additional fluctuations, or clusters, at large spatial scales, which can be seen in Figure 1. For $K = 10$, there is a broad peak at $q \sim 1$, implying some spatial correlation of the clusters. For $K = 1$ and 0.1 there are still signs of peaks at the lowest accessible values of q.

3.2. Dynamics ($C_{max} = 4$). (a) Determination of $f(q,\tau)$. Figure 3a shows the normalized time-averaged intensity correlation functions (ICF) $g_T^{(2)}(q,\tau)$ calculated at $q = 1.31$ ($n_1 = n_2 = 5$ in eq 10) for three different samples (i.e., different bond topologies) with spring constant $K = 10$. At this value of scattering vector the ensemble-averaged scattered intensity (averaged over

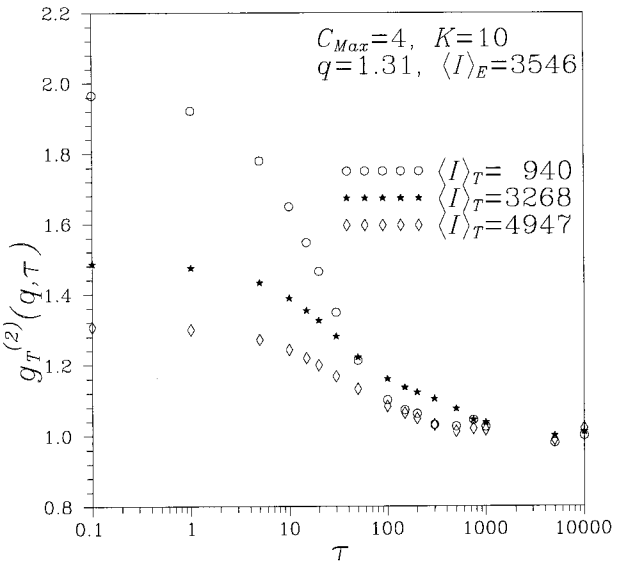

3a

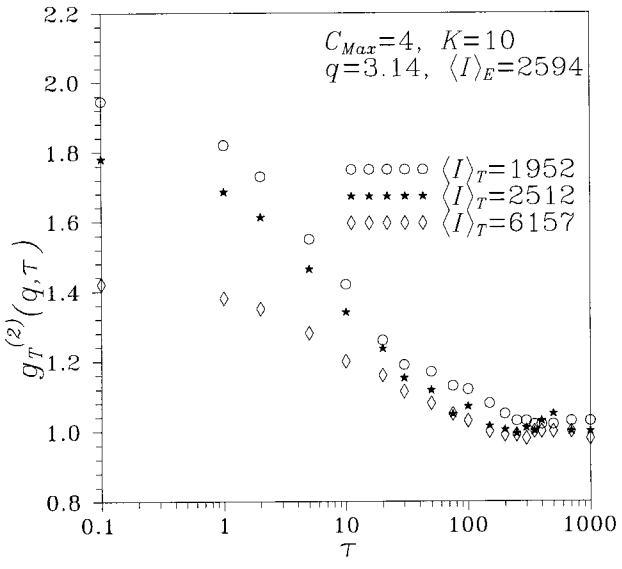

3b

Figure 3. Normalized time-averaged intensity correlation functions $g_T^{(2)}(q,\tau)$ versus correlation delay time τ (measured in time steps and plotted logarithmically) for a gel with connectivity $C_{max} = 4$, spring constant $K = 10$. (a) Scattering vector $q = 1.31$; (b) scattering vector $q = 3.14$. The three curves correspond to data obtained from speckles with different time-averaged intensities $\langle I(q)\rangle_T$; the ensemble-averaged intensities were $\langle I(q)\rangle_E = 3546$ (a) and 2594 (b). Note that in these, and subsequent, plots of time correlation functions the data points corresponding to $\tau = 0$ are actually plotted at $\tau = 0.1$.

64 samples) is $\langle I(q)\rangle_E = 3546$, giving $S(q) = 1.54$ (since $N^2 = 48^2 = 2304$). Because of the different configurations of frozen-in density fluctuations, each of the three samples gives a different speckle pattern of scattered light with different time-averaged intensities,[4,10] $\langle I(q)\rangle_T = 4947$ (bright speckle), $\langle I(q)\rangle_T = 3268$ (speckle of intermediate intensity), and $\langle I(q)\rangle_T = 940$ (dark speckle). It is clear from Figure 3a that different time-averaged ICF's are found for each of the three samples. The same conclusion can be drawn from Figure 3b, which shows ICF's for three samples, also with $K = 10$, at larger

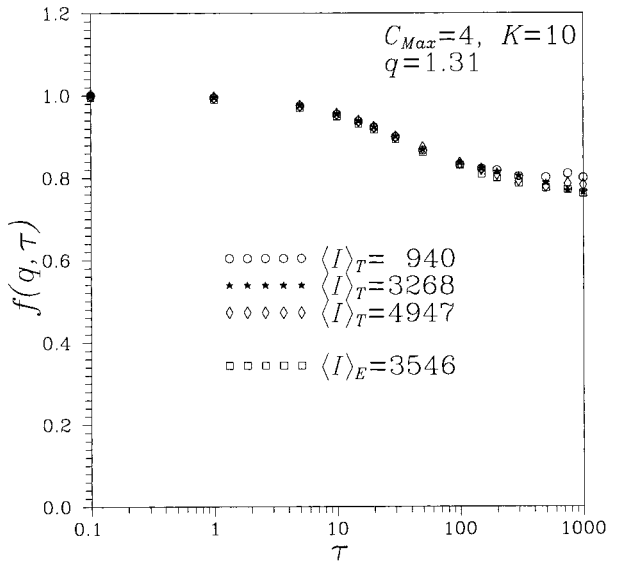

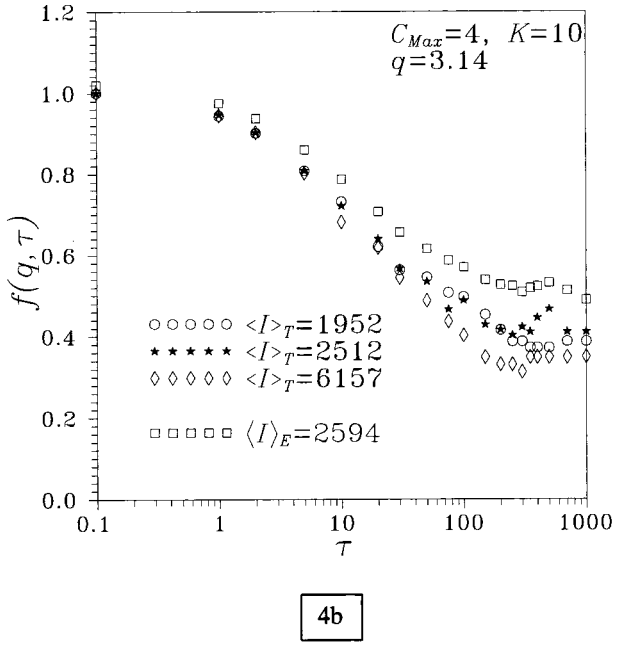

Figure 4. Intermediate scattering functions $f(q,\tau)$ corresponding to the intensity correlation functions of Figure 3. (a) Scattering vector $q = 1.31$; (b) scattering vector $q = 3.14$. Data represented by circles, asterisks, and diamonds were obtained from the equivalent results of Figure 3 using the method of Pusey and van Megen. Data represented by squares were obtained by direct ensemble averaging over 64 samples. See text for further details.

scattering vector, $q = 3.14$ ($n_1 = n_2 = 12$), where $S(q) \sim 1$ (Figure 2).

As described in section 2.3, there are two methods by which the ensemble-averaged intermediate scattering function $f(q,\tau)$ can be obtained from time-averaged measurements. The first is to combine many time-averaged measurements according to eqs 16 and 15. The second is the method of Pusey and van Megen[4,10] (eq 17). The results of applying both these procedures for the data of Figures 3 are shown in Figure 4.

It is evident from eq 17 that, regardless of statistical uncertainties in $g_T^{(2)}(q,\tau)$, $\langle I(q)\rangle_T$, and $\langle I(q)\rangle_E$, the method of Pusey and van Megen gives $f(q,0) = 1$. However, uncertainties in these quantities lead to uncertainties in $f(q,\tau)$ at $\tau \neq 0$. As noted in section 2.4, the uncertainties in $g_T^{(2)}(q,\tau)$ and $\langle I(q)\rangle_T$ are quite small, <3%. Thus, the superposition, observed in Figure 4a, of the three sets of data shown in Figure 3a verifies the identity, predicted by eq 17, of the quantities $\langle I(q)\rangle_T[\sqrt{2-g_T^{(2)}(q,0)} - 1]$ measured for different speckle intensities $\langle I(q)\rangle_T$ (provided that the same value of $\langle I(q)\rangle_E$ is used in each of the three calculations, as it was here). The same comments apply to the data of Figures 3b and 4b. In fact, the superposition of the three data sets in Figure 4a is, coincidentally, rather better than one might expect from the consideration of statistical uncertainties of section 2.4. However, the data of Figure 4b show a statistical spread more in line with expectation.

Also shown in Figure 4a,b are estimates of $f(q,\tau)$ obtained by direct ensemble averaging, eqs 15 and 16. The number of samples used was $M = 64$ so that, as mentioned in section 2.4, the statistical uncertainty in $f(q,\tau)$ calculated in this way is expected to be about 10%. The data of Figure 4b show this degree of uncertainty whereas (again accidentally) precise agreement is seen in Figure 4a.

Thus, to within these uncertainties, the results of Figures 3 and 4 verify that both methods give the same intermediate scattering function $f(q,\tau)$. Furthermore, they provide rather precise validation of the method of Pusey and van Megen (eq 17).

(b) General Behavior of $f(q,\tau)$. Figure 5a shows intermediate scattering functions $f(q,\tau)$, determined as described in the previous section, for a range of scattering vectors (including the data of Figure 4) for the case $C_{max} = 4$, $K = 10$. We concentrated on calculations at $q < 1$, since this corresponds to the limit ($Qa \ll 2\pi$) in which light scattering operates for real gels. (Henceforth, the intermediate scattering functions shown were determined by ensemble averaging, eqs 15 and 16, over 64 samples. In this process the calculated value of $f(q,\tau)$ can show statistical fluctuations of about ±10% around the theoretical value of 1. For clarity, we have normalized the estimated $f(q,\tau)$'s by their zero-time values so that all the displayed intermediate scattering functions start from 1.)

It is evident from that, in general, the intermediate scattering functions $f(q,\tau)$ do not decay to zero, corresponding to a complete decay of density fluctuations, but rather to a nonzero value $f(q,\infty)$, the "nonergodicity parameter", whose magnitude represents the fraction of the fluctuations that are "frozen-in". The magnitude of $f(q,\infty)$ depends on scattering vector and decreases with increasing q.

It can be shown that the ensemble-averaged intensity can be written[4]

$$\langle I(q)\rangle_E = \langle I_F(q)\rangle_E + \langle I_C(q)\rangle_E \tag{20}$$

where $\langle I_F(q)\rangle_E$ and $\langle I_C(q)\rangle_E$ are respectively the fluctuating and static components of the intensity and

$$\langle I_F(q)\rangle_E = \langle I(q)\rangle_E(1 - f(q,\infty)); \quad \langle I_C(q)\rangle_E = \langle I(q)\rangle_E f(q,\infty) \tag{21}$$

Thus, with use of eq 19, we can write

$$S_F(q) = S(q)(1 - f(q,\infty)); \quad S_C(q) = S(q)\, f(q,\infty) \tag{22}$$

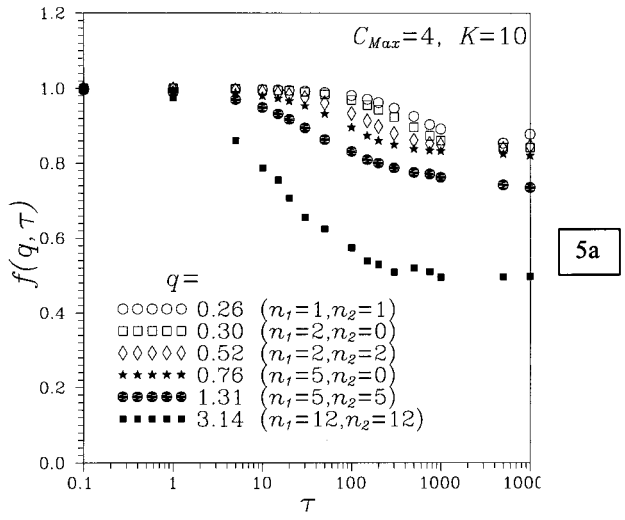

5a

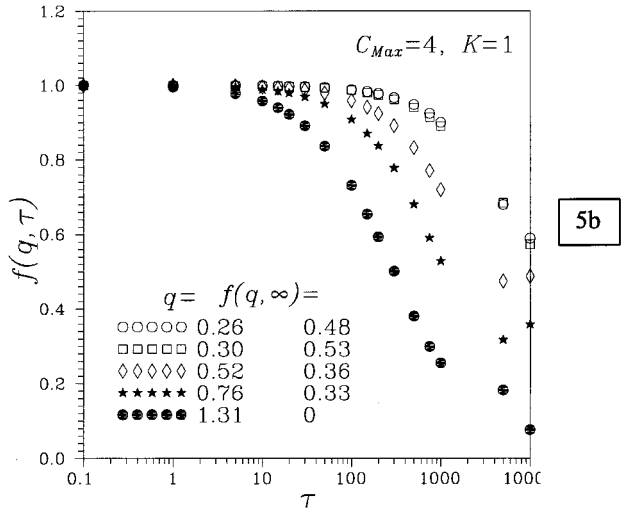

5b

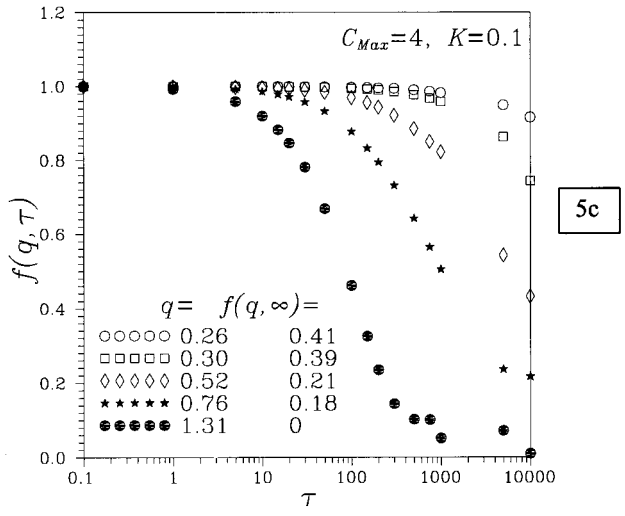

5c

Figure 5. Intermediate scattering functions $f(q,\tau)$, obtained by ensemble averaging 64 samples, for gels with connectivity $C_{max} = 4$ for different values of scattering vector q. (a) Spring constant $K = 10$; (b) $K = 1$; (c) $K = 0.1$. In (b) and (c) the listed values of $f(q,\infty)$ were calculated from eq 18 as discussed in the text.

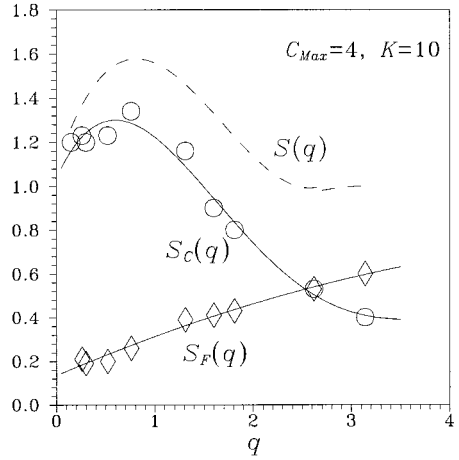

6a

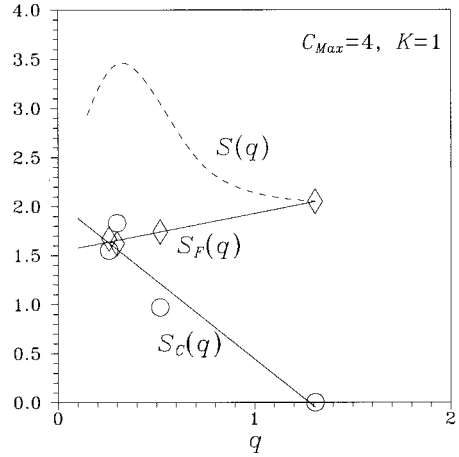

6b

Figure 6. Total static structure factor $S(q)$, its fluctuating part $S_F(q)$, and its constant part $S_C(q)$ versus scattering vector q for a gel with connectivity $C_{max} = 4$. (a) Spring constant $K = 10$; (b) $K = 1$.

where $S_F(q)$ is the "fluctuating" part of the static structure factor, associated with the dynamic density fluctuations, and $S_C(q)$ is the part associated with the frozen-in, or "constant", fluctuations. In Figure 6a we plot $S(q)$, $S_F(q)$, and $S_C(q)$ as functions of q and observe that, over this range of q, $S_F(q)$ is always considerably smaller than the total structure factor $S(q)$ and, in fact, is significantly smaller than 1. It appears, therefore, that this particular model gel ($C_{max} = 4$ and $K = 10$) provides an example of a system that shows intrinsic nonergodicity without the presence of large-scale inhomogeneities (see the discussion of section 1). Thus, the real-space structure (Figure 1b) is fairly homogeneous so that the total static structure factor (Figure 2) does not deviate strongly from 1, yet the dynamics reveal a large frozen-in component (Figure 6).

Starting from the Langevin equation (eq 1) or the equivalent Smoluchowski or many-body diffusion equation, it has so far not proved possible to obtain a theoretical prediction for the full time dependence of the intermediate scattering functions of a system of interacting Brownian particles.[11] However, for the case considered here where hydrodynamic interactions between the scatterers are neglected, it can be shown[11] that the *initial* decay of $f(q,\tau)$ is related simply to the static structure factor $S(q)$. Thus, if we define the

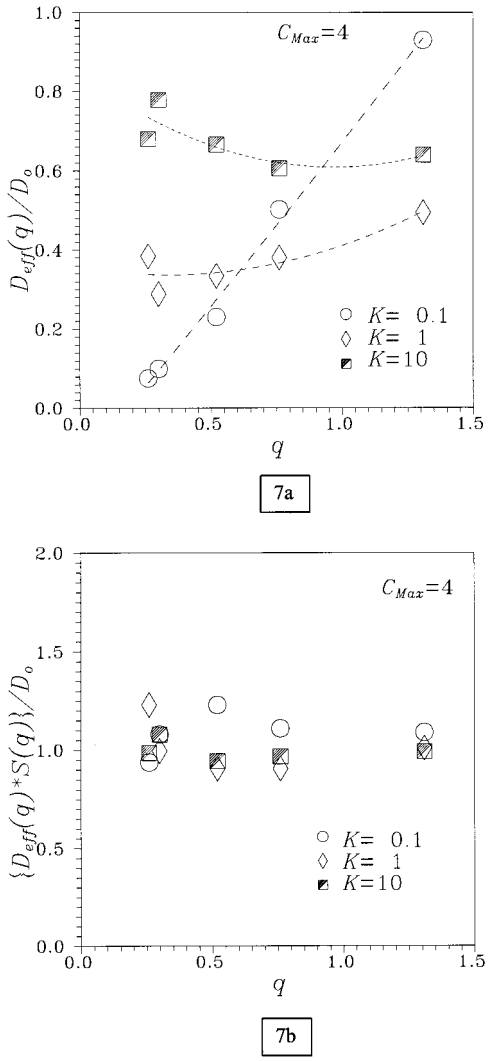

Figure 7. (a) Effective diffusion coefficients $D_{eff}(q)$, normalized by the free-particle diffusion constant D_0, versus scattering vector q for gels with connectivity $C_{max} = 4$ and three different spring constants. (b) The product of the normalized diffusion coefficients of (a) and the static structure factors $S(q)$ versus q.

effective diffusion coefficient $D_{eff}(q)$ associated with this initial decay by

$$D_{eff}(q) = -\frac{1}{q^2}\lim_{\tau\to 0}\frac{d}{d\tau}\ln f(q,\tau) \qquad (23)$$

then theory predicts

$$D_{eff}(q) = \frac{D_0}{S(q)} \qquad (24)$$

where D_0 is the "free-particle" diffusion constant discussed in section 2.2. Figure 7a shows the quantity $D_{eff}(q)/D_0$ for the data of Figure 5a; the effective diffusion coefficients were determined by cumulant analysis[12] of the intermediate scattering functions. Although, for this case ($C_{max} = 4$, $K = 10$), $D_{eff}(q)$ does not show a strong dependence on q, its behavior does mirror that of $S(q)$ (Figures 2 and 6); as seen in Figure 7b, the product $(D_{eff}(q)/D_0)S(q)$ is close to 1, as predicted by eq 24. (Figure 7 also shows other tests of eq 24, to be discussed in the next section, where the effective diffusion coefficient shows much stronger q dependence.)

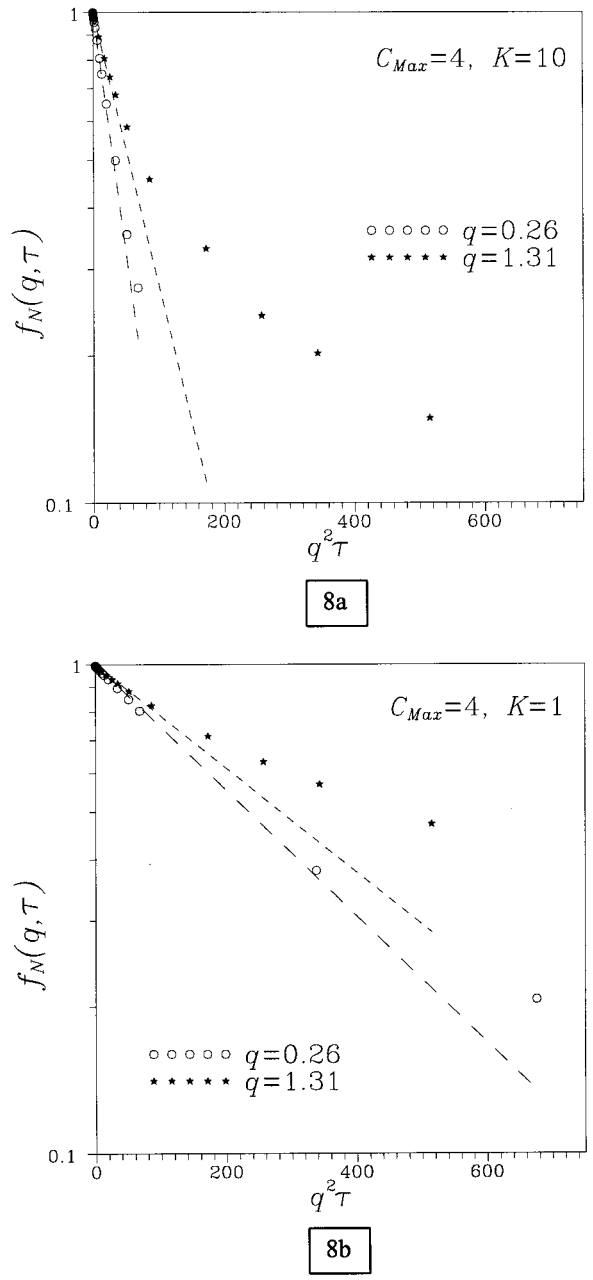

Figure 8. Dynamic parts $f_N(q,\tau)$ (eq 26) of the intermediate scattering functions versus delay time τ (note the logarithmic ordinate and linear abscissa scales) for gels with connectivity $C_{max} = 4$ at two values of scattering vector. (a) Spring constant $K = 10$; (b) $K = 1$.

As noted above, there are no theoretical predictions for the full structure of $f(q,\tau)$. In experiments on polymer gels it is sometimes found[6] that the dynamic part $f_N(q,\tau)$ of $f(q,\tau)$, where

$$f(q,\tau) = f_N(q,\tau)(1 - f(q,\infty)) + f(q,\infty) \qquad (25)$$

so that

$$f_N(q,\tau) = \frac{f(q,\tau) - f(q,\infty)}{1 - f(q,\infty)} \qquad (26)$$

shows a nearly single-exponential decay. Figure 8a shows $f_N(q,\tau)$ for the $q = 0.26$ and 1.31 data of Figure 5a. For $q = 0.26$ the decay is quite exponential (a

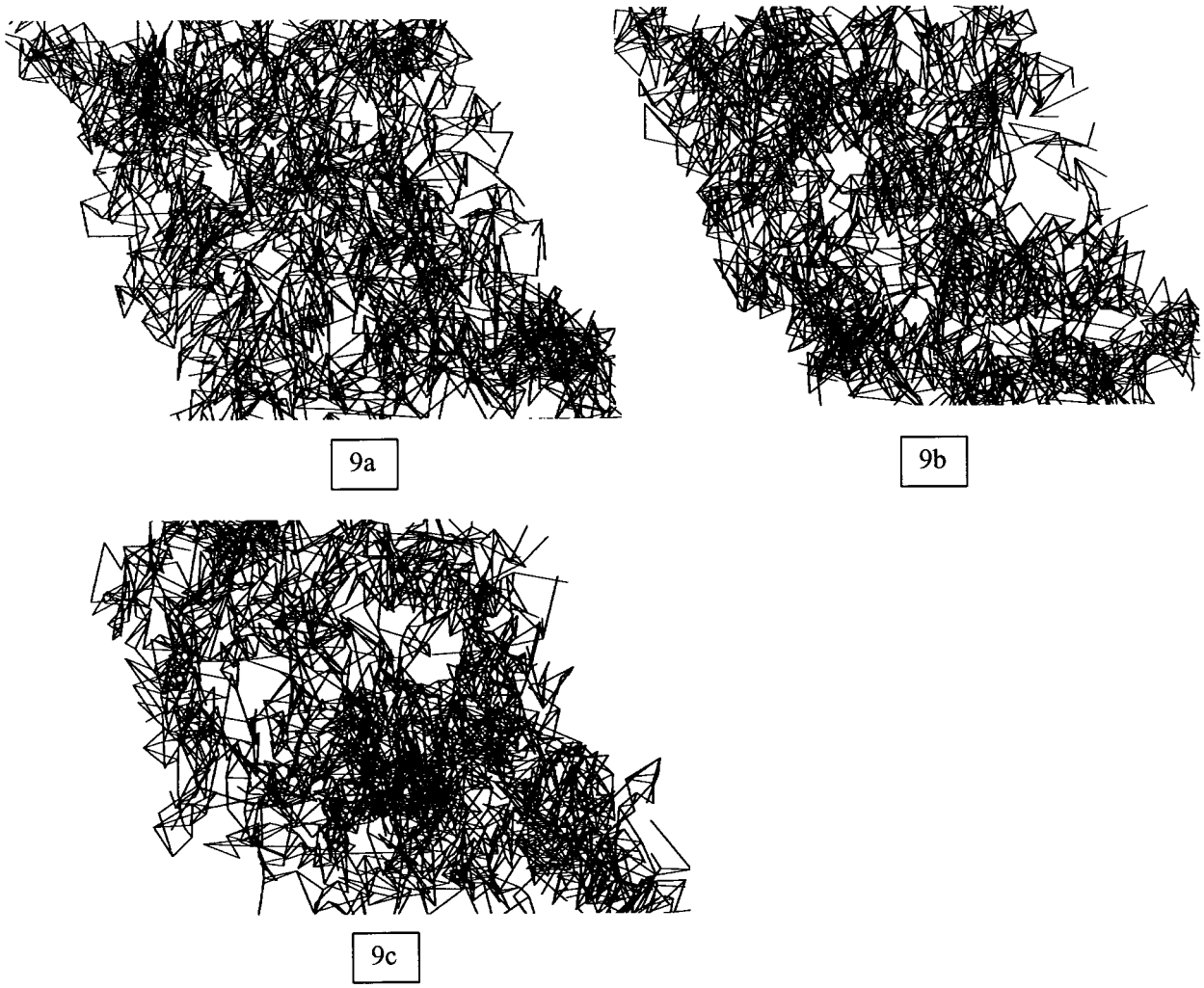

Figure 9. Real-space configurations of a gel with connectivity $C_{max} = 4$ and weak springs, $K = 0.1$, after (a) 1×10^5 time steps, (b) 2×10^5 time steps, and (c) 5×10^5 time steps.

straight line in this log-linear plot) whereas for $q = 1.31$ significant departures from exponentiality are seen.

(c) Comparison of Dynamics with Different Spring Constants. Figure 5 shows intermediate scattering functions for $C_{max} = 4$ and for different values of the spring constant K: Figure 5a, $K = 10$ (already discussed above); Figure 5b, $K = 1$; Figure 5c, $K = 0.1$. Comparing these results, we first note that $f(q,\tau)$ decays more slowly at $q = 0.26$ for $K = 1$ than for $K = 10$, consistent with eq 24 and the larger value of $S(q)$ (see Figure 2). For $K = 0.1$ and $q = 0.26$, where $S(q) \sim 10$, the decay is slower still. Figure 7a shows the effective diffusion coefficients $D_{eff}(q)$ (eq 23) for all three values of spring constant. Figure 7b tests eq 24 and shows that it is satisfied to within ~20% for all the data, including the case $K = 0.1$ where $D_{eff}(q)$ and $S(q)$ vary individually with q by a factor of about 10.

Next we consider the nonergodicity parameters $f(q,\infty)$. We see that some of the scattering functions in Figure 5b,c have not reached plateau values, giving $f(q,\infty)$, in the time window, $\tau < 10\,000$, over which $g_T^{(2)}(q,\tau)$ was computed. However, as pointed out in section 2.3, $f(q,\infty)$ can also be computed, via eq 18, from $g_T^{(2)}(q,0)$, the zero-time value of $g_T^{(2)}(q,\tau)$. Values of $f(q,\infty)$, determined in this way, are listed in Figure 5b,c. For $K = 1$ (Figure 5b) these values are not too different from the $\tau = 10\,000$ values of $f(q,\tau)$, suggesting that the displayed intermediate scattering functions have almost reached their plateaux. For $K = 0.1$ (Figure 5c) the differences are much larger, and one can question whether the fluctuations, especially those at small q, have decayed in the duration, 100 000 time steps, of the computation. To test this conjecture, we performed one longer computation, of duration 500 000 time steps, for the case $C_{max} = 4$ and $K = 0.1$. Figure 9 shows the resulting real-space configurations after 100 000, 200 000, and 500 000 time steps. Between the first two pictures one can sense some correlation, implying incomplete decay of the large-scale density fluctuations over 100 000 time steps. However comparison of parts a and c of Figure 9 shows little correlation, suggesting eventual complete decay of the fluctuations. We conclude, therefore, that for $K = 0.1$ the system is effectively totally ergodic, but that the magnitudes of the fluctuation times are comparable to the duration of the computation so that the scattering functions of Figure 5c show spurious nonergodicity.

Returning to the cases $K = 10$ and 1 (Figure 5), we note that for all scattering vectors the system is more ergodic (i.e., $f(q,\infty)$ is closer to 0) at $K = 1$. Thus, at $q = 0.26$, $f(q,\infty) \sim 0.86$ for $K = 10$ and $f(q,\infty) \sim 0.48$ for $K = 1$. At $q = 1.31$, $f(q,\infty) \sim 0.75$ for $K = 10$, and for $K = 1$ the fluctuations are essentially ergodic, $f(q,\infty) \sim 0$. Figure 6b shows the fluctuating and constant parts of the static structure factor, eq 22, for $K = 1$. In contrast

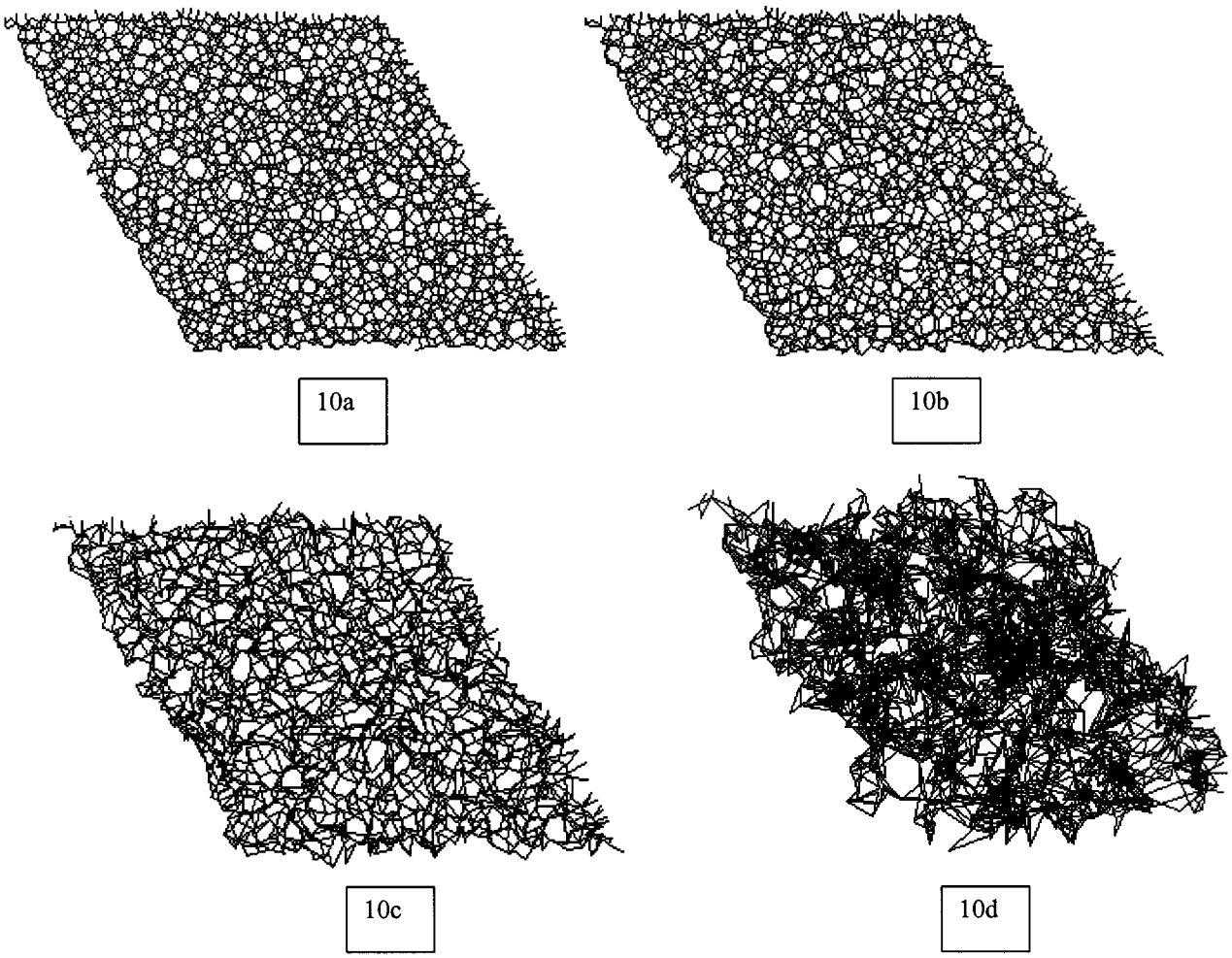

Figure 10. Representations of the real-space structure of a model gel, formed by bond dilution with maximum connectivity $C_{max} = 5$. (a) The relaxed configuration in the absence of Brownian motion. (b−d) The same gel after 10^5 time steps of Brownian motion with three different values of normalized spring constant K: (b) $K = 10$; (c) $K = 1$; (d) $K = 0.1$.

to the situation for $K = 10$ (Figure 6a), $S_F(q)$ is greater than 1 at all scattering vectors.

Figure 8b shows the fluctuating parts $f_N(q,\tau)$ of the scattering functions for $K = 1$ and $q = 0.26$ and 1.31. As for $K = 10$ (see previous section) (Figure 8a), the function is quite exponential at $q = 0.26$ but distinctly nonexponential at $q = 1.31$. At present we cannot explain this behavior.

3.3. Results at Maximum Connectivity $C_{max} = 5$. We now consider briefly simulations for the case of maximum connectivity $C_{max} = 5$. We concentrate on comparison with the results for $C_{max} = 4$, highlighting the similarities and differences.

Figure 10 shows a particular realization of the gel for $C_{max} = 5$: (a) the relaxed configuration; (b−d) snapshots of the configurations after 100 000 time steps of Brownian motion for spring constants $K = 10$, 1, and 0.1, respectively. Figure 11 shows static structure factors (cf. Figure 2 for $C_{max} = 4$), and Figure 12 shows intermediate scattering functions (cf. Figure 5). As for $C_{max} = 4$ (Figure 1b), one can see in the configuration at $K = 10$ remnants of the relaxed structure; however, reflecting the higher connectivity, the structure is more uniform (compare Figures 1b and 10b). Consequently, the structure factor (Figure 11) is smaller and in fact has magnitude considerably less than 1 at all $q < 5$. Similarly, at $K = 1$, the structure for $C_{max} = 5$ (Figure 10c) is more uniform than that for $C_{max} = 4$ (Figure 1c),

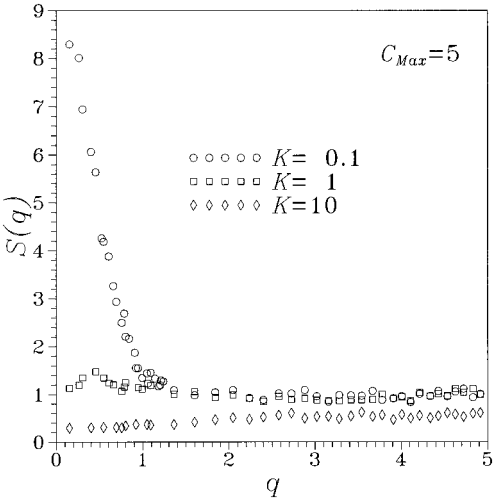

Figure 11. Ensemble-averaged structure factors $S(q)$ versus scattering vector q for gel with maximum connectivity $C_{max} = 5$ and indicated values of the normalized spring constant K.

and the structure factor is again smaller, now having a value close to 1 for all q. At $K = 0.1$, however, the structures for $C_{max} = 5$ and $C_{max} = 4$ look quite similar (Figures 10d and 1d), as do both the structure factors (Figures 11 and 2) and the intermediate scattering functions (Figures 12c and 5c). It is perhaps not surpris-

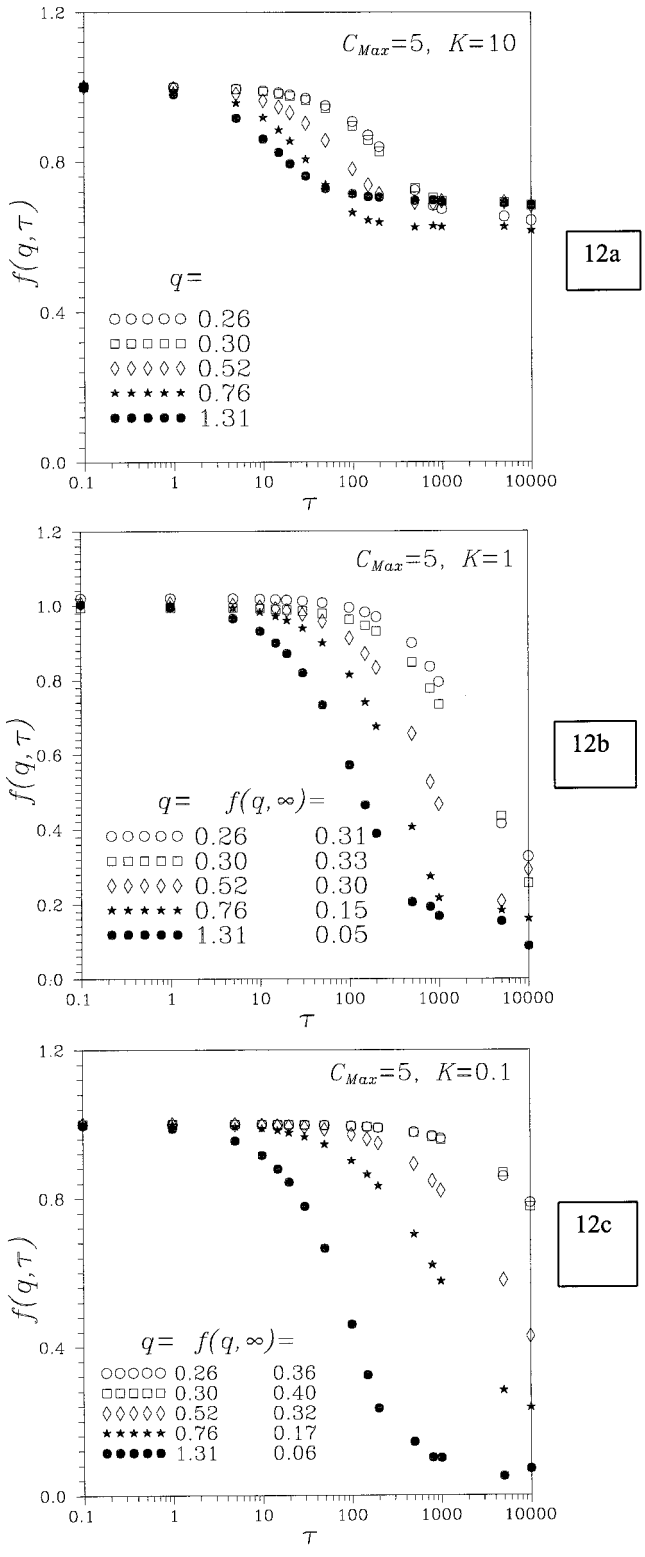

Figure 12. Intermediate scattering functions $f(q,\tau)$ for gels with connectivity $C_{max} = 5$ for different values of scattering vector q. (a) Spring constant $K = 10$; (b) $K = 1$; (c) $K = 0.1$.

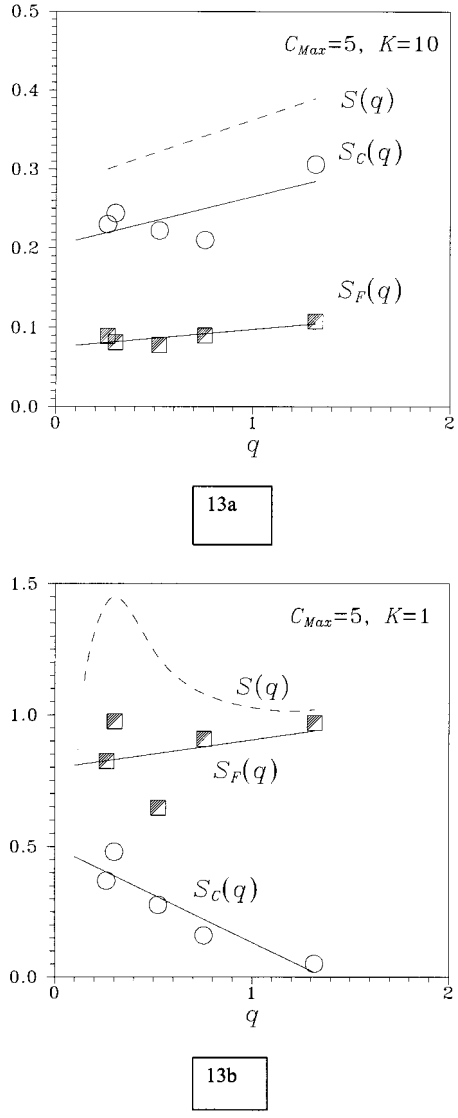

Figure 13. Total static structure factor $S(q)$, its fluctuating part $S_F(q)$, and its constant part $S_C(q)$ versus scattering vector q for gels with connectivity $C_{max} = 5$. (a) Spring constant $K = 10$; (b) $K = 1$.

ing that the behavior of these very loose structures, where vertexes connected by a single spring will typically find themselves separated by 10 lattice spacings, is relatively insensitive to the connectivity. In Figure 13 we give the fluctuating and constant parts of the static structure factor $S(q)$, as well as $S(q)$ itself, for $K = 10$ and 1 and $C_{max} = 5$ (cf. Figure 6 for $C_{max} = 4$). As before, $S_C(q)$ and $S_F(q)$ were calculated using eq 22 from the nonergodicity parameters $f(q,\infty)$ (Figure 12a,b) and the total structure factors (Figure 11).

To interpret these results, it is instructive to consider the scattering by a regular lattice (all vertexes 6-fold connected). A *rigid* regular lattice will scatter only at values of scattering vector Q that correspond to Bragg reflections, the first of which occurs at $q = Qa = 4\pi/\sqrt{3} = 7.26$ for this lattice. However, when the vertexes undergo Brownian motion, thermal diffuse scattering, resulting from the displacement of the vertexes from their equilibrium positions, will be seen at all q. The amplitude of the thermal diffuse scattering will be weak for strong springs and vice versa. Furthermore, the thermal diffuse scattering from a regular lattice is expected to be fully fluctuating, since the average amplitude of the scattered radiation (the amplitude of the radiation scattered by the vertexes in their average, equilibrium, positions) is zero. When some disorder is added to the lattice, for example by random bond dilution, we expect to see some static scattering, associated with the frozen disorder, in addition to the thermal diffuse scattering.

The scattering behavior in the small-q light scattering regime, $q < 1$, seen in Figures 6 and 13 can be understood in terms of these sources of dynamic and static scattering. As mentioned above, for $C_{max} = 6$ (the ordered lattice) only fully fluctuating thermal diffuse scattering is expected. A well-diluted lattice, with $C_{max} = 2$, will also show only fully fluctuating scattering since it corresponds to a polydisperse solution of (2-fold connected) linear chains that are not restrained by cross-links. We therefore expect to find the maximum frozen disorder and static scattering with C_{max} between 2 and 6. Thus, with $K = 10$ and $C_{max} = 5$ (Figure 13a), relatively small static scattering is observed, $S_C(q) \sim 0.20$, consistent with the relatively uniform structure discussed above. However, at $K = 10$ and $C_{max} = 4$ (Figure 6a), $S_C(q) \sim 1.20$, consistent with more disorder. From Figures 6 and 13 we also observe that the dynamic (thermal diffuse) scattering increases as the springs are weakened. Thus, at $C_{max} = 5$, $S_F(q) \sim 0.10$ and ~ 0.90 for $K = 10$ and 1, respectively; at $C_{max} = 4$ the corresponding values are $S_F(q) \sim 0.20$ and ~ 1.50.

4. Concluding Remarks

We have simulated dynamic light scattering by a model "gel" formed by random bond dilution of a two-dimensional triangular lattice of beads connected by springs. The main aims of this work were to elucidate the conditions under which the system shows nonergodicity, the existence of frozen density fluctuations that do not relax completely, and to investigate possible connections between nonergodicity and the existence of density fluctuations of large spatial extent which are observed in many real gels. Our results fulfill these aims only partially. Depending on the choice of parameters, the maximum connectivity C_{max} and the spring constant K, the model systems do indeed exhibit both nonergodicity and large-scale fluctuations; however, there does not appear to be a direct connection between the two. Thus, for $C_{max} = 4$, $K = 10$ and for $C_{max} = 5$, $K = 1$, the gels show little structure ($S(q) \sim 1$) yet clear nonergodicity (e.g., $f(q,\infty) > 0.5$ for $C_{max} = 4$, $K = 10$). On the other hand, for weak springs $K = 0.1$, the gels for both $C_{max} = 4$ and $C_{max} = 5$ show very large density inhomogeneities ($S(q) \sim 10$ at small q) but, we have argued, little or no nonergodicity. Nevertheless, the system that perhaps comes closest to modeling a real gel, $C_{max} = 4$, $K = 1$ (see below), does exhibit both large-scale inhomogeneities and nonergodicity.

A simple picture of a real gel is one formed by instantaneously introducing cross-links into a semidilute solution of linear polymers.[5] Between adjacent cross-links one would then find a segment of unperturbed random-coil polymer. The simple theory of rubber elasticity shows that the energy stored in a random coil whose ends are separated by a distance equal to the unperturbed coil's radius of gyration is of order the thermal energy, k_BT. As discussed in section 2.2, this corresponds roughly to the case $K = 1$ for the model gel. We note that the behavior of the model gel at $C_{max} = 4$, $K = 1$ is similar to that of the poly(acrylamide) gel studied by Joosten et al.[6] at a total polymer concentration by weight of 2.5% and relative cross-link content of 2−3%. In the real experiment, dynamic light scattering operates in the limit $q = Qa \ll 1$. From Figures 2 and 6b we note that, in this limit, the system for $C_{max} = 4$, $K = 1$ has $S(q) \sim 3$, indicating significant density inhomogeneity, with fluctuating component $S_F(q) \sim 1.7$. For the poly(acrylamide) gel Figures 7 and 8 of ref 6 show $S(q) \sim 3$ (the ratio of the light intensity scattered by the gel to that of the un-cross-linked solution) and $S_F(q) \sim 1.3$. While we do not wish to attribute too much significance to this similarity, it does suggest that the model used here is not totally unrealistic. We further note that the model with $K > 1$ might have relevance to a gel swollen from its conditions of preparation, whereas $K < 1$ might correspond to a shrunken gel. A gel composed of charged polymers, where Coulombic repulsions can contribute strongly to the elasticity, might also be modeled by $K > 1$. In fact, some experiments[7] on charged poly(acrylic acid) gels showed no large-scale inhomogeneities but still significant nonergodicity, $f(q,\infty) > 0$, similar to the model with $C_{max} = 4$ and $K = 10$, discussed in section 3.2(b).

As a byproduct of this work we have verified, in a well-defined system, the method of Pusey and van Megen (eq 17) for analyzing dynamic light scattering by nonergodic media (see section 3.2(a)). We have also provided further confirmation of the relationship, eq 24, expected for any system of interacting Brownian particles, between the effective (first cumulant) diffusion coefficient $D_{eff}(q)$ and the static structure factor $S(q)$ (see section 3.2(b)).

Finally, we emphasize again the fact that neglect of excluded volume in our model severely limits its application to real gels (see section 1). Panyukov and Rabin[5] have pointed out that an elastic network in which excluded volume is neglected has many possible states of equilibrium but that only one such state exists when excluded volume is "switched on". This observation might well account for the large dynamic clusters observed in our model at small spring constant $K = 0.1$ (sections 3.1, 3.2(c), and 3.3).

Acknowledgment. This research was supported in part by the European Commission TRACS Program at Edinburgh Parallel Computing Centre and by the UK Biotechnology and Biological Sciences Research Council.

Appendix. Statistical Uncertainties in Ensemble Averaging

An estimate of the normalized ensemble-averaged intensity correlation function is obtained by combining M individual measurements of the time-averaged intensity and intensity correlation function according to eq 16. We wish to calculate the uncertainty in such an estimate. For simplicity, we will assume that the measurement time is long enough that good time averages are obtained, i.e., that the uncertainty in time-averaged quantities can be neglected (however, see section 2.4 for further discussion). Thus, we are interested solely in the uncertainty in the ensemble-averaged quantities arising from the finiteness of M.

Using a shorthand notation, we define

$$\hat{G}(\tau) = \frac{1}{M}\sum_{p=1}^{M}\langle I_p(0)\, I_p(\tau)\rangle_T \qquad \text{(A1)}$$

as the estimated unnormalized intensity correlation function,

$$\hat{I} = \frac{1}{M}\sum_{p=1}^{M}\langle I_p(t)\rangle_T \qquad \text{(A2)}$$

as the estimated average intensity, and

$$E \equiv \hat{g}_E^{(2)}(q,\tau) = \frac{\hat{G}(\tau)}{\hat{I}^2} \tag{A3}$$

as the desired estimate of the normalized intensity correlation function. Here, as in section 2.3, p labels the topology of the sample. Writing the estimates in terms of deviations about their ensemble-averaged values, indicated by $\langle\cdots\rangle$, we have[13]

$$E = \frac{\langle\hat{G}\rangle\left[1+\frac{\delta\hat{G}}{\langle\hat{G}\rangle}\right]}{\langle\hat{I}\rangle^2\left[1+\frac{\delta\hat{I}}{\langle\hat{I}\rangle}\right]^2} = \frac{\langle\hat{G}\rangle}{\langle\hat{I}\rangle^2}\left\{1 - 2\frac{\delta\hat{I}}{\langle\hat{I}\rangle} + 3\frac{(\delta\hat{I})^2}{\langle\hat{I}\rangle^2} + \frac{\delta\hat{G}}{\langle\hat{G}\rangle} - 2\frac{\delta\hat{I}\,\delta\hat{G}}{\langle\hat{I}\rangle\langle\hat{G}\rangle} + \cdots\right\} \tag{A4}$$

Thus, we get average values

$$\langle E\rangle = \frac{\langle\hat{G}\rangle}{\langle\hat{I}\rangle^2}\left\{1 + 3\frac{\langle(\delta\hat{I})^2\rangle}{\langle\hat{I}\rangle^2} - 2\frac{\langle\delta\hat{I}\,\delta\hat{G}\rangle}{\langle\hat{I}\rangle\langle\hat{G}\rangle} + \cdots\right\} \tag{A5}$$

$$\langle E^2\rangle = \frac{\langle\hat{G}\rangle^2}{\langle\hat{I}\rangle^4}\left\{1 + 10\frac{\langle(\delta\hat{I})^2\rangle}{\langle\hat{I}\rangle^2} - 8\frac{\langle\delta\hat{I}\,\delta\hat{G}\rangle}{\langle\hat{I}\rangle\langle\hat{G}\rangle} + \frac{\langle(\delta\hat{G})^2\rangle}{\langle\hat{G}\rangle^2} + \cdots\right\} \tag{A6}$$

so that the variance in the estimated normalized ensemble-averaged intensity correlation function is

$$\frac{\langle(\delta E)^2\rangle}{\langle E\rangle^2} \equiv \frac{\langle E^2\rangle}{\langle E\rangle^2} - 1 = 4\frac{\langle(\delta\hat{I})^2\rangle}{\langle\hat{I}\rangle^2} - 4\frac{\langle\delta\hat{I}\,\delta\hat{G}\rangle}{\langle\hat{I}\rangle\langle\hat{G}\rangle} + \frac{\langle(\delta\hat{G})^2\rangle}{\langle\hat{G}\rangle^2} + \cdots \tag{A7}$$

To evaluate the various quantities in eq A7, we recognize that the amplitude of the instantaneous electric field scattered in topology p can be written[4]

$$E_p(t) = E_{p\mathrm{F}}(t) + E_{p\mathrm{C}} \tag{A8}$$

Here $E_{p\mathrm{F}}(t)$ is the fluctuating component of the scattered field; it varies randomly in time and has the same zero-mean complex Gaussian statistical properties for all p.[4] The constant component of the scattered field, $E_{p\mathrm{C}}$, is independent of time but has different values for different topologies p; over the ensemble of all possible topologies it is also a zero-mean complex Gaussian variable.[4] The instantaneous scattered intensity can be written

$$I_p(t) \equiv |E_p(t)|^2 = I_{p\mathrm{F}}(t) + E_{p\mathrm{F}}(t)\,E^*{}_{p\mathrm{C}} + E^*{}_{p\mathrm{F}}(t)\,E_{p\mathrm{C}} + I_{p\mathrm{C}} \tag{A9}$$

where $I_{p\mathrm{F}}(t) \equiv |E_{p\mathrm{F}}(t)|^2$ and $I_{p\mathrm{C}} = |E_{p\mathrm{C}}{}^2|$. Assuming a long averaging time (above) and exploiting the statistical properties of the fields described above, the time average of eq A9 becomes

$$\langle I_p(t)\rangle_T = I_{\mathrm{F}} + I_{p\mathrm{C}} \tag{A10}$$

where I_{F} is the time or ensemble average of $I_{p\mathrm{F}}(t)$. Similarly

$$\langle I_p(0)\,I_p(\tau)\rangle_T = \langle I_{\mathrm{F}}(0)\,I_{\mathrm{F}}(\tau)\rangle + 2I_{\mathrm{F}}I_{p\mathrm{C}} + 2I_{p\mathrm{C}}\langle E_{\mathrm{F}}(0)\,E^*{}_{\mathrm{F}}(\tau)\rangle + I_{p\mathrm{C}}{}^2 = I_{\mathrm{F}}{}^2[1 + g_{\mathrm{F}}{}^2(\tau)] + 2I_{\mathrm{F}}I_{p\mathrm{C}}[1 + g_{\mathrm{F}}(\tau)] + I_{p\mathrm{C}}{}^2 \tag{A11}$$

where

$$g_{\mathrm{F}}(\tau) \equiv \frac{\langle E_{\mathrm{F}}(0)\,E^*{}_{\mathrm{F}}(\tau)\rangle}{I_{\mathrm{F}}} \tag{A12}$$

(and time or ensemble averages are the same for properties of $E_{\mathrm{F}}(t)$).

From eq A10 we get

$$\hat{I} = I_{\mathrm{F}} + \frac{1}{M}\sum_{p=1}^{M} I_{p\mathrm{C}} \tag{A13}$$

so that

$$\langle\hat{I}\rangle = I_{\mathrm{F}} + I_{\mathrm{C}} = I \tag{A14}$$

where I_{F}, I_{C} ,and I are respectively the ensemble-averaged values of the fluctuating, constant, and total intensities. Similarly,

$$\langle\hat{I}^2\rangle = I_{\mathrm{F}}{}^2 + 2I_{\mathrm{F}}I_{\mathrm{C}} + \frac{1}{M^2}\sum_{p=1}^{M}\sum_{q=1}^{M}\langle I_{p\mathrm{C}}I_{q\mathrm{C}}\rangle = I^2 + \frac{I_{\mathrm{C}}{}^2}{M} \tag{A15}$$

since

$$\langle I_{p\mathrm{C}}I_{q\mathrm{C}}\rangle = \langle I_{\mathrm{C}}\rangle^2(1 - \delta_{pq}) + \langle I_{\mathrm{C}}\rangle^2\delta_{pq} \tag{A16}$$

and $\langle I_{\mathrm{C}}^2\rangle = 2\langle I_{\mathrm{C}}\rangle^2$ for a Gaussian field. Thus

$$\frac{\langle(\delta\hat{I})^2\rangle}{\langle\hat{I}\rangle^2} = \frac{\langle\hat{I}^2\rangle}{\langle\hat{I}\rangle^2} - 1 = \frac{1}{M}\frac{I_{\mathrm{C}}{}^2}{I^2} \tag{A17}$$

By similar, but increasingly tedious, manipulations it can be shown that

$$\frac{\langle\delta\hat{I}\,\delta\hat{G}\rangle}{\langle\hat{I}\rangle\langle\hat{G}\rangle} = \frac{2I_{\mathrm{C}}{}^2}{M}\frac{I + I_{\mathrm{F}}g_{\mathrm{F}}(\tau) + I_{\mathrm{C}}}{I^3 + I[I_{\mathrm{F}}g_{\mathrm{F}}(\tau) + I_{\mathrm{C}}]^2} \tag{A18}$$

and

$$\frac{\langle(\delta\hat{G})^2\rangle}{\langle\hat{G}\rangle^2} = \frac{4I_{\mathrm{C}}{}^2}{M}\frac{[I_{\mathrm{F}}(1 + g_{\mathrm{F}}(\tau)) + I_{\mathrm{C}}]^2 + 2I_{\mathrm{C}}[I_{\mathrm{F}}(1 + g_{\mathrm{F}}(\tau)) + 2I_{\mathrm{C}}]}{\{I^2 + [I_{\mathrm{F}}g_{\mathrm{F}}(\tau) + I_{\mathrm{C}}]^2\}^2} \tag{A19}$$

Using eqs A17−19 in eq A7 then gives the required uncertainty in the ensemble-averaged intensity correlation function for arbitrary delay time τ. For simplicity, we will evaluate these results only in the limits $\tau = 0$ and $\tau = \infty$ using $g_{\mathrm{F}}(0)$ and $g_{\mathrm{F}}(\infty) = 0$. From section 2.2-(b) we note that

$$\frac{I_{\mathrm{C}}}{I} = f, \quad \frac{I_{\mathrm{F}}}{I} = 1 - f, \quad \text{where } f \equiv f(q,\infty) \tag{A20}$$

Thus, eqs A17−A19 become

$$\frac{\langle(\delta\hat{I})^2\rangle}{\langle\hat{I}\rangle^2} = \frac{f^2}{M} \tag{A21}$$

$$\frac{\langle\delta\hat{I}\,\delta\hat{G}\rangle}{\langle\hat{I}\rangle\langle\hat{G}\rangle} = \frac{2f^2}{M} \text{ for } \tau = 0, \quad = \frac{2f^2}{M}\frac{1+f}{1+f^2} \text{ for } \tau = \infty \tag{A22}$$

$$\frac{\langle(\delta\hat{G})^2\rangle}{\langle\hat{G}\rangle^2} = \frac{f^2}{M}(4+f^2) \text{ for } \tau = 0,$$

$$= \frac{4f^2}{M}\frac{1+2f+2f^2}{(1+f^2)^2} \text{ for } \tau = \infty \tag{A23}$$

Combining eqs A21−A23 in eq A7 gives

$$\frac{\langle(\delta E)^2\rangle^{1/2}}{\langle E\rangle} = \frac{f^2}{M^{1/2}} \text{ for } \tau = 0,$$

$$= \frac{2f^2}{M^{1/2}}\frac{(f^2-2f+2)^{1/2}}{1+f^2} \text{ for } \tau = \infty \tag{A24}$$

From eq 15 we see that the estimated intermediate scattering function $\hat{f}(q,\tau)$ is given by

$$\hat{f}(q,\tau) = \sqrt{\hat{g}_E^{(2)}(q,\tau) - 1} \tag{A25}$$

so that its relative uncertainty is

$$\frac{\delta\hat{f}(q,\tau)}{\hat{f}(q,\tau)} = \frac{g_E^{(2)}(q,\tau)}{2[g_E^{(2)}(q,\tau) - 1]}\frac{\delta\hat{g}_E^{(2)}(q,\tau)}{\hat{g}_E^{(2)}(q,\tau)} \tag{A26}$$

where the relative uncertainty in $\hat{g}_E^{(2)}(q,\tau)$ is given by eq A24 (see also eq A3).

As an example, we evaluate eq A26 for $M = 64$ and the two cases (see Figure 4): (a) $f(q,\infty) = 0.8$, $g_E^{(2)}(q,0) = 2$, $g_E^{(2)}(q,\infty) = 1.64$; (b) $f(q,\infty) = 0.4$, $g_E^{(2)}(q,0) = 2$, $g_E^{(2)}(q,\infty) = 1.16$. Case a gives relative uncertainties in the intermediate scattering function of 0.08 at $\tau = 0$ and 0.13 at $\tau = \infty$; for case b the equivalent results are 0.02 and 0.15.

References and Notes

(1) Candau, S. J.; Young, C. Y.; Tanaka, T. *J. Chem. Phys.* **1979**, *70*, 4694.
(2) Geissler, E. In *Dynamic Light Scattering*; Brown, W., Ed.; Oxford University Press: New York, 1993; p 471.
(3) Tanaka, T.; Hocker, L. O.; Benedek, G. B. *J. Chem. Phys.* **1973**, *59*, 151.
(4) Pusey, P. N.; van Megen, W. *Physica A* **1989**, *157*, 705. Pusey, P. N. *Macromol. Symp.* **1994**, *79*, 17.
(5) Panyukov, S.; Rabin, Y. *Phys. Rep.* **1996**, *269*, 1; *Macromolecules* **1996**, *29*, 7960.
(6) Joosten, J. G. H.; McCarthy, J. L.; Pusey, P. N. *Macromolecules* **1991**, *24*, 6690.
(7) Moussaïd, A.; Candau, S. J.; Joosten, J. G. H. *Macromolecules* **1994**, *27*, 2102.
(8) Grimson, M. J. *Mol. Phys.* **1991**, *74*, 1097.
(9) Ermak, D. L. *J. Chem. Phys.* **1975**, *62*, 4189−96.
(10) Joosten, J. G. H.; Gelade, E.; Pusey, P. N. *Phys. Rev. A* **1990**, *42*, 2161.
(11) Pusey, P. N. In *Liquids, Freezing and the Glass Transition*; Levesque, D., Hansen, J.-P., Zinn-Justin, J., Eds.; North-Holland: Amsterdam, 1991; p 763.
(12) Koppel, D. E. *J. Chem. Phys.* **1972**, *57*, 4814. Brown, J. C.; Pusey, P. N.; Deitz, R. *J. Chem. Phys.* **1975**, *62*, 1136.
(13) Saleh, B. *Photoelectron Statistics*; Springer-Verlag: Berlin, 1978.

MA981159N